Journal of Physical Science, Vol. 28(1), 27–47, 2017

Synthesis, Crystal Structure and Vibrational Spectral Analysis of Guanidinium Hydrogen L-aspartate Single Crystal

Uma Devi Thangaraj,[1*] Meenakshi Rajagantham,[2] Kalpana Govindarajulu[3] and Josephine Prabha Arulsamy[4]

[1]Department of Physics, Government Arts College for Women (Autonomous), Pudukkottai, 622001, India
[2]Department of Physics, Cauvery College for Women, Trichy, Tamil Nadu, 620018, India
[3]Department of Physics, K. Ramakrishnan College of Engineering, Kariyamanikam Road, Trichy, 621112, India
[4]Department of Physics, Bishop Heber College (Autonomous), Trichy, 620017, India

[*]Corresponding author: kavin_shri@yahoo.co.in

Published online: 15 April 2017

To cite this article: Thangaraj, U. D. et al. (2017). Synthesis, crystal structure and vibrational spectral analysis of guanidinium hydrogen L-aspartate single crystal. *J. Phys. Sci.*, 28(1), 27–47, https://doi.org/10.21315/jps2017.28.1.3

To link to this article: https://doi.org/10.21315/jps2017.28.1.3

ABSTRACT: *Single crystals of guanidinium hydrogen L-aspartate (GULAS), a salt of guanidine derivative, have been grown by slow-cooling method and characterised by infrared (IR) spectroscopy, powder and single-crystal x-ray powder diffraction (XRD). From the vibrational spectral analysis, the spectral band assignment is carried out to identify the various functional groups in GULAS. After arriving at the equilibrium geometry, the analysis of intramolecular charge transfer interactions using natural bond orbital (NBO) method, first order hyperpolarisability, molecular electrostatic potential and frontier molecular orbitals have been carried out using density functional theory. The second-order NLO response is also studied using Kurtz and Perry powder method.*

Keywords: Single crystal, slow cooling method, XRD, FTIR, guanidinium hydrogen

1. INTRODUCTION

Second harmonic generation (SHG) is one of the most interesting phenomena observed in non-centrosymmetric crystals and is widely utilised for optical

frequency conversion and modulation. Crystals of all amino acids except glycine, owing to the presence of chiral carbon atom and non-centrosymmetry, serve as candidate for non-linear optical (NLO) materials,[1] widely used in SHG and ultimately in generating blue green lasers.[2] Our recent research work is mostly centred around NLO materials, which are amino acid derivatives obtained from glycine, L-proline, etc.[3,4] In addition to the ease of growing by slow evaporation solution technique (SEST), the characteristics of amino acid crystals can be modified using molecular engineering and chemical synthesis.[5]

Guanidines are the imido derivatives of urea, with one imine and two amine units. Guanidine derivatives are versatile intermediates used in the manufacture of plastics, resins, rubber chemicals, photo chemicals, fungicides and disinfectants in industries and many of their complexes are potential NLO materials.[6–12] The solid-state complexation of guanidine with different organic acids such as aspartic acid, oxalic acid, etc. has an interesting aspect concerning the weak hydrogen bonds of N–H…O and O–H…O.[13–16]

Guanidinium hydrogen L-aspartate (GULAS) is one which consists of guanidinium and aspartate ions, connected by strong N–H…O hydrogen bonds. It crystallises in the orthorohmbic structure having four molecules per unit cell, with a noncentrosymmetric space group $P2_12_12_1$. Though Krumbe and Haussühl have reported the detailed structural and physical properties of GULAS, the spectral analysis has not been reported in open literature.[17] Hence, in the present study, an attempt is made to grow and characterise GULAS using Fourier-transform infrared (FTIR) spectroscopy. In order to support the experimental outcomes, the detailed vibrational spectral investigations using the scaled quantum mechanical (SQM) force field technique based on density functional theory (DFT) calculations is performed. Additionally, from the natural bond orbital analysis (NBO), electron charge transfer through intermolecular hydrogen bonding is explained.

2. EXPERIMENTAL

The stoichiometric portions of guanidinium carbonate and an aqueous solution of L-aspartic acid are made to react to synthesise GULAS. The reactants are thoroughly dissolved in double distilled water and stirred well, using a temperature-controlled magnetic stirrer to yield a homogeneous mixture of solution. Upon slow evaporation at room temperature, transparent crystalline salt of GULAS are obtained. Purification of the synthesised salt is done by repeated recrystallisation process. The chemical structure of GULAS is shown in Figure 1.

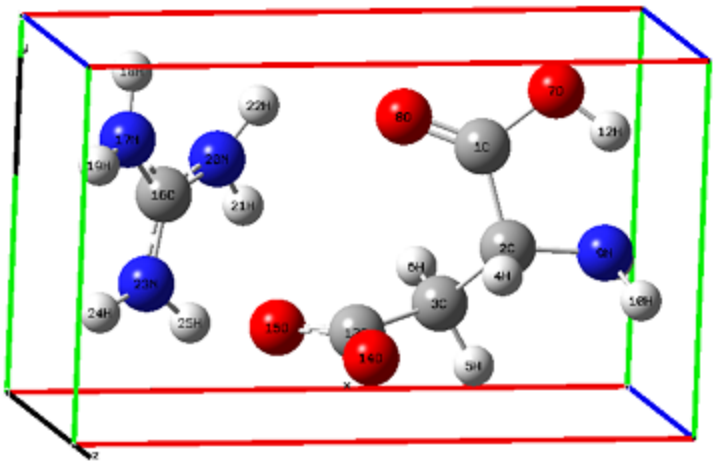

Figure1: Optimised structure of GULAS.

The reaction mechanism is as follows:

$$C_2H_7N_3O_3 + C_4H_7NO_4 \rightarrow [CN_3H_6]C_4H_6NO_4 + H_2O_+CO_2$$

Saturated solution of GULAS is prepared at 35°C from recrystallised salt and filtered with microfilters. About 200 ml of this solution is taken in a beaker and placed in a constant temperature bath having a temperature accuracy of ± 0.01°C. Single crystal of GULAS is grown by the slow cooling method by reducing the temperature from 35°C at the rate of 0.1°C per day. Well-developed crystals of size 15 × 5 × 3 mm^3 are harvested in a growth period of 15 days and one such is shown in Figure 2.

Structural analysis is carried out using powder and single crystal XRD (Enraf Nonius–CAD4) and the spectroscopic analysis using FTIR. All DFT calculations are performed with the Gaussian 09 program.[18] The geometries were fully optimised in the gas phase at DFT levels by B3LYP functions, which combine Becke's three-parameter exchange function (B3) with the correlation function of Lee, Yang and Parr (LYP). Upon optimisation, all of the complexes worked out to have non-imaginary frequency geometries. These theoretical findings confirmed that the optimised structure of GULAS correspond to real minima on the potential energy surface, thus ensuring stability.

Figure 2: As-grown GULAS single crystal.

3. STRUCTURAL ANALYSIS

3.1 X–ray Diffraction Studies

The GULAS crystals are transparent and non-hygroscopic, with well-developed facial morphology (Figure 2). The single crystal XRD study shows that it crystallises in the orthorhombic crystal system with the lattice parameters as shown in Table 1.

Table 1: Orthorhombic lattice parameters of GULAS obtained from single crystal XRD.

S. No.	a (Å)	b (Å)	c (Å)	Reference
1.	5.067	9.509	16.822	Present Work
2.	5.073	9.513	16.842	17

The optimised geometrical parameters such as bond lengths and bond angles obtained at B3LYP/6-311G (d,p) level are given in Table 2.

Table 2: Experimental and theoretical geometric data for GULAS at B3LYP/6-311G (d,p) level.

Bond length (Å)		XRD	Bond angles (º)		XRD
Guanidinium ion[19]					
C16-N17	1.3604	1.325	N17-C16-N20	119.86	121.1
C16-N20	1.3395	1.312	N20-C16-N23	118.7039	118.8
C16-N23	1.3336	1.330	N17-C16-N23	121.4309	120
N17-H18	1.0034	0.94			
N17- H19	1.003	1.03			
N20-H21	1.025	1			
N20-H22	1.0093	1.09			
N23-H24	1.004	0.85			
N23-H25	1.0529	0.65			
L-aspartate ion[18]					
C1-C2	1.5352	1.537	C13-O14-015	125.7721	126.7
C2-C3	1.5383	1.526	C2-C3-C13	110.97	114.4
C3-C13	1.5402	1.526	C1-C2-C3	112.8789	112.5
C13-O14	1.263	1.252	C1-C2-O7	113.2218	118.9
C13-O15	1.3089	1.2572			
C3-H5	1.0938	0.95			
C3-H6	1.0889	1.02			
C2-H4	1.095	0.95			
C2-N9	1.486	1.492			
N9-H10	1.0112	0.91			
N9-H11	1.0139	0.94			

The calculated theoretical values are in good agreement with the corresponding experimentally reported values.[17,19] Powder X-Ray diffraction pattern of GULAS is given in Figure 3.

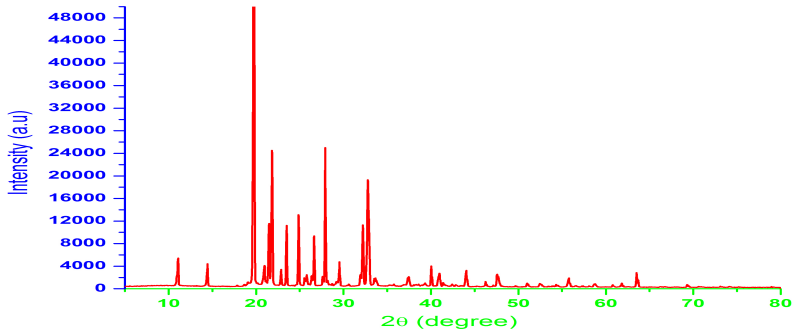

Figure 3: Powder x-ray diffraction pattern of GULAS.

3.2 Vibrational Analysis

Vibrational analysis of GULAS is made on the basis of aspartate and guanidinium groups. The recorded FTIR spectrum of GULAS is shown in Figure 4.

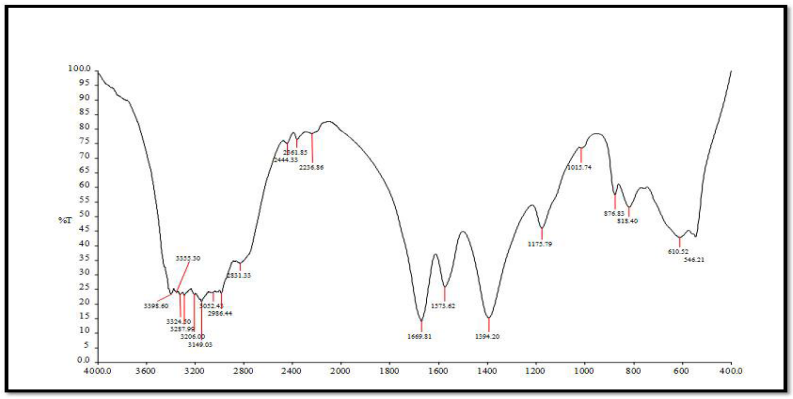

Figure 4: FTIR spectrum of GULAS.

The FTIR band observed at 3397 cm^{-1} is assigned as vibration due to NH_2 asymmetric stretch of guanidine group. The in-plane O-H deformation vibration usually appears as a strong band in the region 1440–1200 cm^{-1}. The strong band at 1348 cm^{-1} in the IR spectrum corresponds to the vibrations due to C-O-H in-plane bending. As the carboxylic group vibrations due to the C=O stretching are usually expected in the range 1725–1655 cm^{-1},[20,21] the band appearing at 1674 cm^{-1} for GULAS is assigned to the C=O stretching vibrations. At 1007 and 892 cm^{-1}, the

vibrations respectively correspond to CH_{2scis} and CH_{2rock}. Few other in-plane and out of plane bending vibrations are assigned as shown in Table 3.

Table 3: Observed and calculated wave numbers (cm^{-1}) for GULAS at B3LYP/6-311G (d,p) level.

Wavenumber (cm^{-1})		Assignments
FTIR	Calculated	
3397	3312	NH_2 asymmetric stretch
3097	3099	C-H stretching vibrations
1674	1769	C=O asymmetric stretch
1578	1572	COO stretching vibration
1490	1425	C-H in plane bending vibration
1348	1394	O-H in plane deformation vibration
1301	1304	C-N-H bending vibrations
1226	1229	C-N-H bending vibrations
1156	1181	C-N-H bending vibrations
1061	1051	CC in- plane bending vibration
1007	1011	CC in- plane bending vibration
892	894	CH_{2scis}
844	850	CH_{2rock}
823	804	C-H out of plane bending vibration
751	729	CC out of plane bending vibration
619	639	CC out of plane bending vibration
582	585	CC out of plane bending vibration
532	539	CN-out-of-plane bending modes

It is to be noted that the theoretically computed band values agrees well with the experimental result.

3.3 Analysis of Fukui Indices

The Fukui functions (f(r)) are often used as indices to the local reactivity aiding to analyse the active atomic sites. The Fukui functions (f (r)) measure the change in the electron density of an N electron system upon addition (f^+(r)) or removal (f^-(r)) of an electron. Atom condensed Fukui functions using the Mulliken population

analysis (MPA) and the finite difference (FD) approximations approach introduced by Yang and Mortier[22] were calculated using the equations:

$$f_k^n = q_k(\mathrm{N}+1) - q_k(\mathrm{N}) \text{ for nucleophilic attack} \quad (1)$$

$$f_k^e = q_k(\mathrm{N}) - q_k(\mathrm{N}-1) \text{ for electrophilic attack and} \quad (2)$$

$$f_k^r = \frac{1}{2}\left(q_k(\mathrm{N}+1) - q_k(\mathrm{N}-1)\right) \text{ for radical attack} \quad (3)$$

where $q_k(\mathrm{N}+1)$, $q_k(\mathrm{N})$ and $q_k(\mathrm{N}-1)$ are the electron densities of the (N+1), *N* and (N–1) electron systems, respectively, and measure its electrophilic and nucleophilic tendencies respectively. The Fukui indices calculated for GULAS are listed in Table 4.

Table 4: Condensed Fukui functions for GULAS.

Atom	$q_k(\mathrm{N}+1)$	$q_k(\mathrm{N})$	$q_k(\mathrm{N}-1)$	f_k^n	f_k^e	f_k^r
C 1	0.459903	0.604904	0.669064	–0.145001	–0.064160	–0.104581
C 2	–0.207824	–0.225117	–0.218745	0.017293	–0.006372	0.005460
C 3	–0.398827	–0.439682	–0.450314	0.040855	0.010632	0.025744
H 4	0.138195	0.266375	0.273019	–0.128180	–0.006644	–0.067412
H 5	0.141355	0.201600	0.264566	–0.060245	–0.062966	–0.061606
H 6	0.154588	0.188184	0.232351	–0.033596	–0.044167	–0.038882
O 7	–0.649075	–0.543581	–0.504698	–0.105494	–0.038883	–0.072189
O 8	–0.658377	–0.432675	–0.470598	–0.225702	0.037923	–0.093890
N 9	–0.754045	–0.787299	–0.766058	0.033254	–0.021241	0.016007
H 10	0.293349	0.322035	0.350404	–0.028686	–0.028369	–0.028528
H 11	0.252554	0.312608	0.337172	–0.060054	–0.024564	–0.042309
H 12	0.333880	0.396555	0.422158	–0.062675	–0.025603	–0.044139
C 13	0.446871	0.483096	0.551720	–0.036225	–0.068624	–0.052425
O 14	–0.517634	–0.481659	–0.238603	–0.035975	–0.243056	–0.139516

(*continued on next page*)

Table 4: (*continued*)

Atom	$q_k(\mathrm{N}+1)$	$q_k(\mathrm{N})$	$q_k(\mathrm{N}-1)$	f_k^n	f_k^e	f_k^r
O 15	–0.620100	–0.622037	–0.338633	0.001937	–0.283404	–0.140734
C 16	0.818316	0.963463	1.047818	–0.145147	–0.084355	–0.114751
N 17	–0.778347	–0.810132	–0.825022	0.031785	0.014890	0.048338
H 18	0.350941	0.354811	0.372589	–0.003870	–0.017778	–0.010824
H 19	0.276992	0.345518	0.373069	–0.068526	–0.027551	–0.048039
N 20	–0.733381	–0.765063	–0.812716	0.031682	0.047653	0.039668
H 21	0.333420	0.375533	0.405838	–0.042113	–0.030305	–0.036209
H 22	0.347009	0.349684	0.361156	–0.002675	–0.011472	–0.007073
N 23	-0.756823	–0.783467	–0.810675	0.026644	0.027208	0.026926
H 24	0.288218	0.324401	0.364193	–0.036183	–0.039792	–0.037988
H 25	0.368842	0.401946	0.410944	–0.033104	–0.008998	–0.021051

The most susceptible sites for nucleophilic and electrophilic attacks are identified by these Fukui indices. The charge distributions point out that N20 is the preferred active site for reaction with nucleophilic species and C3 with electrophilic species. The pictorial representations of these indices are shown in Figure 5.

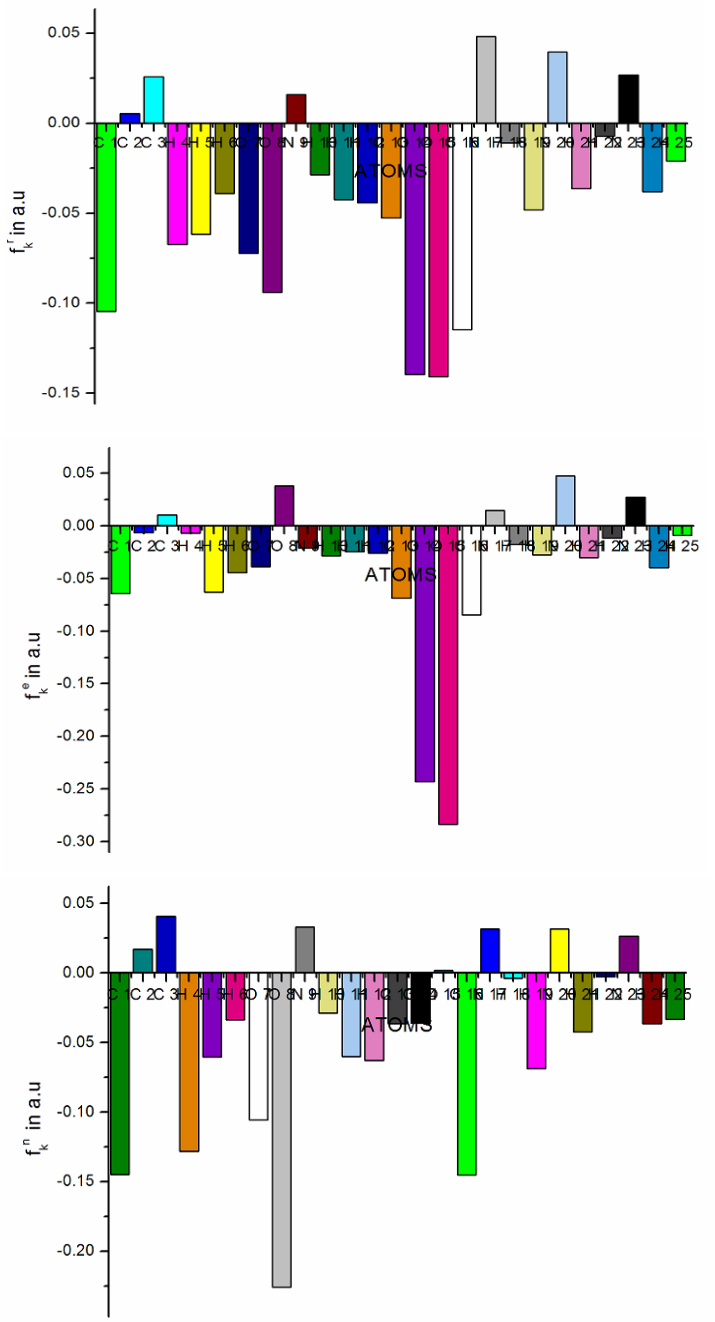

Figure 5: The pictorial representations of Fukui indices of GULAS.

3.4 HOMO-LUMO Analysis

HOMO and LUMO are the main orbitals taking part in chemical reactions. The HOMO and LUMO energy characterises the ability of electron giving and electron accepting, respectively. The energy gap between HOMO and LUMO elucidates the kinetic stability, chemical reactivity, optical polarisability and chemical hardness–softness of a molecule. This is also utilised by the frontier electron density for prediction of the most reactive position in π-electron systems and also explains several types of reaction in conjugated systems. Surfaces for the frontier orbitals were drawn to recognise the bonding scheme of present compound. The positive phase is red and the negative one is green. The pictorial representations of the HOMO-LUMO of GULAS (in neutral, cationic and anionic geometries) are shown in Figure 6.

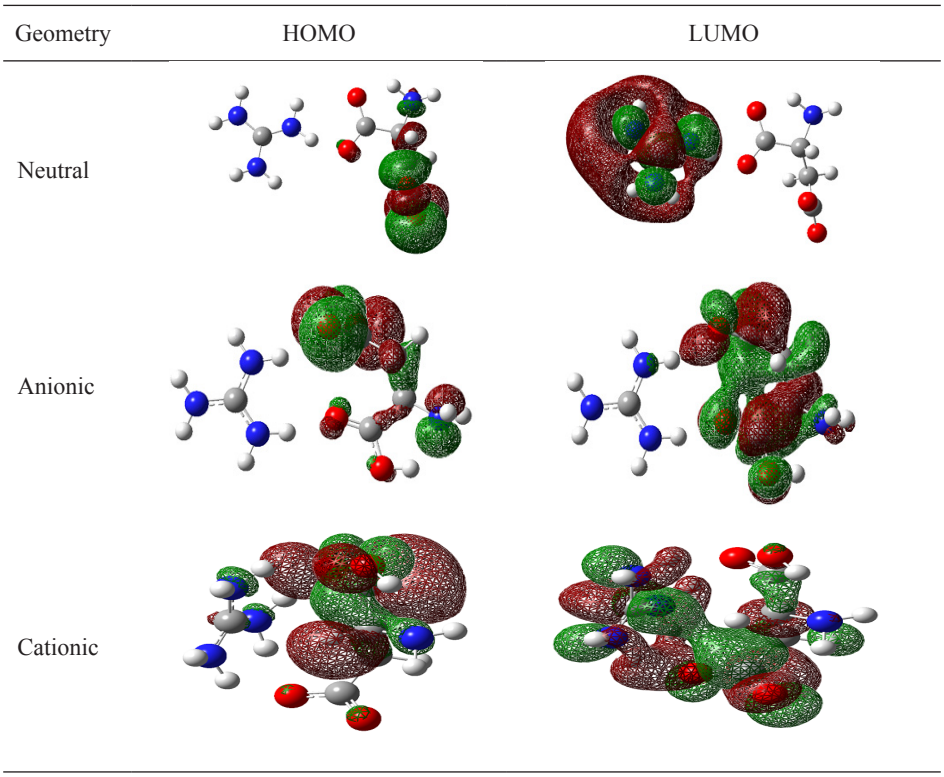

Figure 6: The pictorial representations of HOMO-LUMO of GULAS (in neutral, cationic and anionic geometries).

HOMO is localised on the part of L-aspartate group, whereas LUMO is distributed over the entire guanidine group.

HOMO energy = − 8.9169 eV

LUMO energy = − 2.9088 eV

HOMO–LUMO gap = 6.0081 eV

Gauss-Sum 2.2 Program was used to calculate group contributions to the molecular orbitals (HOMO and LUMO) and prepare the density of states (DOS) spectrum in Figure 7.

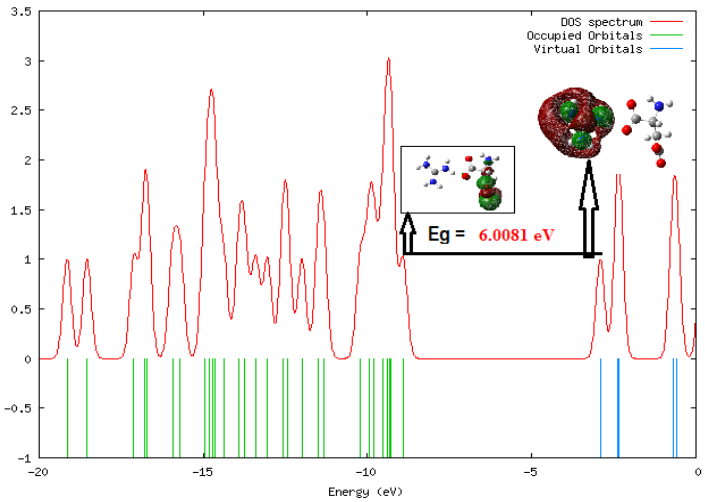

Figure 7: DOS spectrum of GULAS.

The DOS spectrum was formed by convoluting the molecular orbital information with GAUSSIAN curves of unit height. The green and blue lines in the DOS spectrum indicate the HOMO and LUMO levels, respectively. The DOS spectrum also supports the energy gap calculated by HOMO-LUMO analysis. The molecule having large and small energy gaps are referred as hard and soft molecule, respectively. The hard molecule is not more polarisable in comparison with the soft ones because they require immense energy for excitation. The calculated HOMO-LUMO energies and energy gap for GULAS are listed in Table 5.

Table 5: Global reactivity descriptors of GULAS under the applications of electric field.

Parameters	Values			
	No field	Field = 0.0005 a.u	Field = 0.001 a.u	Field = 0.002 a.u
HOMO Energy	−8.9169	−8.988	−9.0378	−8.8986
LUMO Energy	−2.9088	−2.9988	−3.0384	−3.1212
Energy gap	6.0081	5.9892	5.9994	5.7774
Ionisation potential (I)	8.9169	8.988	9.0378	8.8986
Electron affinity (A)	2.9088	2.9988	3.0384	3.1212
Chemical hardness (η)	3.004	2.9946	2.9997	2.8887
Chemical Potential (μ)	−5.9128	−5.9934	−6.0381	−6.0099
Softness (S)	0.1664	0.1669	0.1666	0.1730
Electrophilicity index (ω)	5.8191	5.9976	6.0772	6.2517
Nucleofugality (ΔE_n)	8.7279	8.9965	9.1156	9.3729
Electrofugality (ΔE_e)	14.736	14.9857	15.1151	15.1504
Charge Transfer (ΔN_{max})	1.9683	2.0014	2.0129	2.0804

3.5 Global Reactivity Descriptors under the Electric Field Influences

Absolute hardness and softness are the important properties to measure the molecular stability and reactivity. It is apparent that the chemical hardness fundamentally signifies the resistance towards the deformation or polarisation of the electron cloud of the atoms, ions or molecules under small perturbation of the chemical reaction.

Using Koopman's theorem for closed-shell compounds, hardness (η), softness (S) and the chemical potential (μ) can be defined as follows:

$$\eta = \frac{I - A}{2} \tag{4}$$

$$S = \frac{1}{2\eta} \tag{5}$$

$$\mu = \frac{-(I + A)}{2} \tag{6}$$

where I and A are the ionisation potential and electron affinity of the compounds, respectively. Electron affinity refers to the capability of a ligand to accept precisely one electron from a donor. Ionisation energy is a fundamental descriptor of the chemical reactivity of atoms and molecules. High ionisation energy indicates high

stability of chemical inertness and small ionisation energy indicates high reactivity of the atoms and molecules. Parr et al. have defined a new descriptor to quantify the global electrophilic power of the compound as electrophilicity index (ω), which defines a quantitative classification of the global electrophilic nature of a compound.[23] ω, referred as a measure of energy lowering due to maximal electron flow between donor and acceptor is defined as follows:

$$\omega = \frac{\mu^2}{2\eta} \tag{7}$$

The significance of this new reactivity quantity has been recently demonstrated in understanding the toxicity of various pollutants in terms of their reactivity and site selectivity. The calculated value of electrophilicity index describes the biological activity of GULAS. All the calculated values of hardness, potential, and electrophilicity index are summarised in Table 5.

The maximum amount of the electronic charge that an electrophilic system may accept is given by the following equation:

$$\Delta N_{max} = -\frac{\mu}{\eta} \tag{8}$$

The maximum charge transfer ΔN_{max} in the direction of the electrophile is predicted using Equation 8 which describes the tendency of the molecule to acquire additional electronic charge from the environment. A similar effect as in the electrophilicity index is observed for maximum charge transfer. The charge transfer increases as the field increases (Table 5).

The two new reactivity indices to quantify the nucleophilic and electrophilic capabilities of leaving group are nucleofugality (ΔE_n) and electrofugality (ΔE_e) and they are defined as follows:

$$\Delta E_n = EA + \omega = \frac{(\mu + \eta)^2}{2\eta} \tag{9}$$

$$\Delta E_e = IP + \omega = \frac{(\mu - \eta)^2}{2\eta} \tag{10}$$

All the calculated reactivity descriptors are presented in Table 5.

3.6 Molecular Electrostatic Potential (MESP) Analysis

The molecular electrostatic potential, V(r), at a given point r (x, y, z) in the surrounding area of a molecule, is defined in terms of the interaction energy between the electrical charge generated from the electrons of molecule and a positive test charge (a proton) located at r. The molecular electrostatic potential (MESP) is related to the electronic density and is a very helpful descriptor in determining sites for electrophilic and nucleophilic attacks as well as hydrogen-bonding interactions. To predict reactive sites for electrophilic and nucleophilic attack for the title molecule, MEP was calculated at the B3LYP/6-311G optimised geometry. The negative (red) regions of MEP were related to electrophilic reactivity and the positive (blue) regions to nucleophilic reactivity as shown in Figure 8.

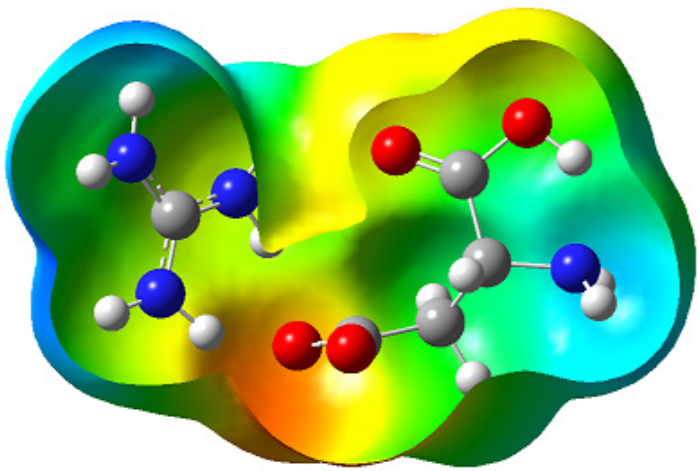

Figure 8: MESP surfaces of GULAS.

The negative electrostatic potential region is observed around the oxygen atoms of CO_2 and carboxylic groups. A maximum positive region is localised on the carbon and hydrogen atoms indicating a possible site for nucleophilic attack.

3.7 Electron Migration Analysis

The NBO analysis is carried out by examining all possible interactions between "filled" (donor) Lewis-type NBOs and "empty" (acceptor) non-Lewis NBOs, and estimating their important stabilising energies by 2nd order perturbation theory. Since these interactions lead to loss of occupancy from the localised NBOs of the idealised Lewis structure into the empty non-Lewis orbitals, they are referred to

as delocalisation corrections to the zeroth-order natural Lewis structure. For each donor NBO (i) and acceptor NBO (j) with delocalisation i → j $E^{(2)}$ is estimated as:

$$E^{(2)} = \Delta E_{ij} = q_i \frac{F(i,j)^2}{\varepsilon_j - \varepsilon_i} \quad (11)$$

where q_i is the donor orbital occupancy ε_j and ε_i are diagonal elements orbital energies and F (i, j) is the off diagonal NBO Fock matrix element. The larger $E^{(2)}$ value, the more intensive is the interaction between electron donors and acceptors, i.e., the more donation tendency from electron donors to electron acceptors and the greater the extent of conjugation of the whole system. DFT level computation is used to investigate the various second-order interactions between the filled orbitals of one subsystem and vacant orbitals of another subsystem, which is a measure of the delocalisation or hyper-conjugation.

Table 6: NBO analysis of second order perturbation theory of Fock matrix of GULAS at B3LYP/6-311G (d,p) level.

Donor(i)	Acceptor(j)	E(2) Kcal/mol	E(j)–E(i) a.u	F(i,j) a.u
n_2 (O15)	σ*(C3 – C13)	13.69	0.65	0.085
n_2 (O15)	σ *(C13 – O14)	8.53	0.77	0.074
n_2 (O15)	σ *(C13 – O14)	3.81	0.34	0.034
n_3 (O15)	σ *(C13 – O14)	4.34	0.73	0.054
n_3 (O15)	π*(C 13 – O14)	69.43	0.29	0.129
n_3 (O15)	σ *(C13 – O15)	19.56	0.67	0.110
n_1 (N17)	σ *(C16 – N23)	51.58	0.25	0.110
n_1 (N20)	σ *(C 16 – N 23)	98.87	0.22	0.138
n_1 (N20)	σ *(N 20 – H22)	5.67	0.68	0.060

As seen from Table 6, the strong interactions can be observed in guanidinium and aspartate moieties. In the guanidinium ion the lone pair n_1(N20) presents the electron-transfer potentials of 98.87kcal/mol to σ*(C16 – N23). In aspartate moiety, the electrons of n_3 (O15) can be redistributed into π*(C13 – O14) with the potential of 69.43 kcal/mol. These two interactions stabilise the GULAS due to the highest stabilisation energies.

3.8 Thermodynamic Properties

On the basis of vibrational analysis, the statistically thermodynamic functions such as heat capacity ($C^0_{p,m}$), entropy (S^0_m), and enthalpy changes (H^0_m) for GULAS were obtained from the theoretical harmonic frequencies and listed in Table 7.

Table 7: Thermo dynamical parameters of GULAS at B3LYP/6-311G (d,p) level.

T (K)	S (J/mol.K)	Cp (J/mol.K)	ΔH (kJ/mol)
100.00	342.85	107.29	7.25
200.00	436.11	169.00	21.06
298.15	514.60	227.33	40.54
300.00	516.01	228.39	40.96
400.00	589.20	281.77	66.54
500.00	657.08	326.78	97.04
600.00	720.02	363.60	131.62
700.00	778.41	393.77	169.53
800.00	832.68	418.88	210.20
900.00	883.27	440.09	253.18
1000.00	930.61	458.24	298.12

From this table, it can be observed that these thermodynamic functions are increasing with temperature ranging from 100 to 1000 K due to the fact that the molecular vibrational intensities increase with temperature and shown in Figure 9.

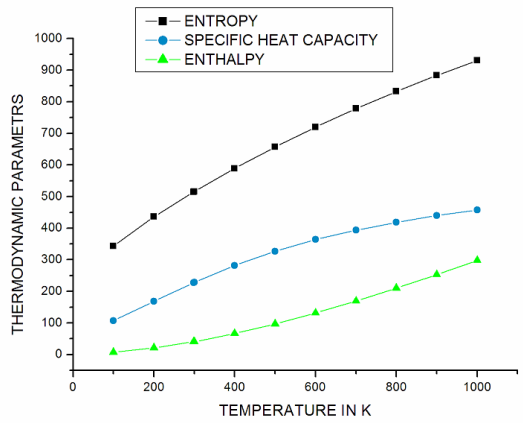

Figure 9: Thermodynamical parameters of GULAS.

3.9 Powder SHG Measurement

The study of nonlinear optical conversion efficiency has been carried out using the modified experimental setup of Kurtz and Perry.[24] A Q-switched Nd:YAG laser beam of wavelength 1,064 nm, with an input power of 2.8 mJ, and pulse width of 8 ns with a repetition rate of 10 Hz was used. The grown single crystal of GULAS was powdered with a uniform particle size and then packed in a microcapillary of uniform bore and exposed to laser radiations. The output from the sample was monochromated to collect the intensity of 532 nm component. The generation of the second harmonics was confirmed by the emission of green light. A sample of potassium dihydrogen phosphate (KDP), also powdered to the same particle size as the experimental sample, was used as a reference material in the present measurement. The SHG conversion efficiency of GULAS is found to be about 0.5 times that of KDP (Table 8).

Table 8: SHG signal energy output.

Input power mJ/pulse	KDP mV	GULAS V
2.8	18	0.094

This may be due to the molecular structure of GULAS in which the main bonds stem from hydrogen bridges between nitrogen atoms of the guanidinium group to oxygen atoms of aspartate group. The N. . . H . . .O distances vary from 2.82 to 2.91 Å with the aspartate. Further, there exists one N . . . H . . . O bond [2.91Å] between the nitrogen atom of each aspartate ion and an oxygen atom of another aspartate ion are the reasons for the SHG efficiency possessed by this material.

4. CONCLUSION

Single crystal of GULAS has been grown. The optimised geometrical parameters were studied. Vibrational spectral analysis has been carried out using FTIR and DFT methods. The Fukui indices analysis points out that N20 is the preferred active site for reaction with nucleophilic species and C3 with electrophilic species through the analysis of Fukui indices. The theoretically calculated small HOMO–LUMO gap explains the extent of intramolecular charge transfer interactions. From the calculated values of DFT based global reactivity descriptors the charge transfer increases under the influence of the electric field. The MESP analysis predicts that the negative regions are mainly localised on oxygen atoms of CO_2 and carboxylic groups and maximum positive region is localised on the carbon

and hydrogen atoms. NBO analysis confirms the presence of hydrogen bonding and investigates the stability as well as the intervening orbital interactions. The thermodynamic parameters are increasing with temperature ranging from 100 to 1000 K. The second-order NLO response was evaluated with the Kurtz and Perry powder method to test its SHG efficiency.

5. ACKNOWLEDGEMENTS

One of the authors T. Uma Devi thanks University Grants Commission for the financial support under minor research project (grant no. MRP 5164/14(SERO/UGC).

6. REFERENCES

1. Senthil, A. et al. (2009). Unidirectional growth of largest L-LMHCl dehydrate crystal by SR method. *J. Cryst. Growth*, 311, 544–547, https://doi.org/10.1016/j.jcrysgro.2008.09.056.
2. Ramesh Kumar, G. et al. (2006). Influence of isoelectric pH on the growth linear and nonlinear optical and dielectric properties of i-threonine single crystals. *Cryst. Growth Des*., 6(6), 1308–1310, https://doi.org/10.1021/cg050438g.
3. Uma Devi, T. et al. (2008). Growth and characterization of glycine picrate single crystal. *Spectrochim. Acta A*, 71, 340–343, https://doi.org/10.1016/j.saa.2007.12.048.
4. Uma Devi, T. et al. (2008). Growth and characterization of l-prolinium picrate single crystal: A promising NLO crystal. *J. Cryst. Growth*, 310, 116–123, https://doi.org/10.1016/j.jcrysgro.2007.10.011.
5. Uma Devi, T. et al. (2009). Synthesis, crystal growth and characterization of l-proline lithium chloride monohydrate: A new semiorganic nonlinear optical material. *Cryst. Growth Des.*, 9, 1370–1374, https://doi.org/10.1021/cg800589m.
6. Drozd, M. & Dudzic, D. (2012). The guanidine and maleic acid (1:1) complex: The additional theoretical and experimental studies. *Spectrochim. Acta A*, 89, 243–251, https://doi.org/10.1016/j.saa.2011.12.069.
7. Drozd, M. & Baran, J. (2006). Polarized vibrational studies of bisguanidinium hydrogenphosphate monohydrate. *Spectrochim. Acta Part A*, 64, 73–86, https://doi.org/10.1016/j.saa.2005.07.001.

8. Drozd, M. (2006). The equilibrium structures, vibrational spectra, NLO and directional properties of transition dipole moments of diguanidinium arsenate monohydrate and diguanidinium phosphate monohydrate: The theoretical DFT calculations. *Spectrochim*. *Acta A*, 65, 1069–1086, https://doi.org/10.1016/j.saa.2006.02.007.
9. Drozd, M., Dudzic, D. & Pietraszko, A. (2013). Crystal structure, differential scanning calorimetric, infrared spectroscopy and theoretical studies of $C(NH_2)_2(NH)^*CH_2{=}{=}CHCOOH$ noncentrosymmetric crystal. *Spectrochim. Acta A Mol. Biomol. Spectrosc*., 105, 135–148, https://doi.org/10.1016/j.saa.2012.12.013.
10. Russell, V. A., Etter, M. C. & Ward, M. D. (1994). Guanidinium para-substituted benzenesulfonates: Competitive hydrogen bonding in layered structures and the design of nonlinear optical materials. *Chem. Mater*., 6, 1206–1217, https://doi.org/10.1021/cm00044a019.
11. Arumanayagam, T. & Murugakoothan, P. (2011). Studies on optical and mechanical properties of new organic NLO crystal: Guanidinium 4-aminobenzoate (GuAB). *P. Mater. Lett.*, 65, 2748–2750, https://doi.org/10.1016/j.matlet.2011.05.081.
12. Sivashankar, V., Siddheswaran, R. & Murugakoothan, P. (2011). Synthesis, growth, structural, optical and thermal properties of a new semiorganic nonlinear optical guanidinium perchlorate single crystal. *Mater. Chem. Phys*., 130, 323–326, https://doi.org/10.1016/j.matchemphys.2011.06.053.
13. Ekaterina, V. et al. (2006). Chiral three-dimensional microporous nickel aspartate with extended Ni−O−Ni bonding. *J. Am. Chem. Soc.*, 128, 9957–9962, https://doi.org/10.1021/ja062743b.
14. Fleck, M., Emmerich, R. & Bohatý, L. (2010). Crystal structure of caesium hydrogen (*L*)- aspartate and an overview of crystalline compounds of aspartic acid with inorganic constituents. *Cryst. Res. Tech.*, 45, 883–887, https://doi.org/10.1002/crat.201000129.
15. Zyss, J. et al. (1993). Synthesis and crystal structure of guanidinium l-monohydrogentartrate: Encapsulation of an optically nonlinear octupolar cation. *Acta Crystall.*, B49, 334–342, https://doi.org/10.1107/S0108768192008395.
16. Anupama, G. & Sanguramath, R. A. (2008). Three-dimensional hybrid networks based on aspartic acid. *J. Chem. Sci.*, 120, 217–222, https://doi.org/10.1007/s12039-008-0025-0.
17. Krumbe, W. & Haussühl, Z. (1987). Structure and physical properties of orthorhombic guanidinium phthalate $[CN_3H_6]_2C_8H_4O_4$ and guanidinium hydrogen l-aspartate $[CN_3H_6]C_4H_6NO_4$. *Kristallogr.*, 179, 267–279, https://doi.org/10.1524/zkri.1987.179.1-4.267.
18. Frisch, M. J. et al. (2009). *Gaussian 09W*. Wallingford: Gaussian.

19. Adams, J. M. (1978). The crystal structure of guanidinium hydrogen oxalate monohydrate. *Acta Cryst.*, B34, 1218–1220, https://doi.org/10.1107/s0567740878005245.
20. George, S. (2001). *Infrared and Raman characteristic group wavenumbers, tables and charts.* Chichester: Wiley.
21. Lin-Vien, D. et al. 1991. *The hand book of infrared and Raman characteristic frequencies of organic molecules*. New York: Academic Press.
22. Yang, W. & Mortier, W. J. (1986). The use of global and local molecular parameters for the analysis of the gas-phase basicity of amines. *J. Am. Chem. Soc*., 108, 5708–5711, https://doi.org/10.1021/ja00279a008.
23. Parr, R. G., Szentpaly, L. V. & Liu, S. J. (1999). Electrophilicity index. *Am. Chem. Soc.,* 121, 1922–1924, https://doi.org/10.1021/ja983494x.
24. Kurtz, S. K. & Perry, T. T. (1986). A powder technique for the evaluation of nonlinear optical materials. *J. Appl. Phys*., 39, 3798, https://doi.org/10.1063/1.1656857.